J Inorg Organomet Polym (2013) 23:409–417
DOI 10.1007/s10904-012-9796-3

Synthesis and Characterization of Catalytically Activity Fe_3o_4–3-Aminopropyl-triethoxysilane/Pd Nanocomposite

E. Karaoglu · M. M. Summak · A. Baykal · H. Sözeri · M. S. Toprak

Received: 15 August 2012 / Accepted: 31 October 2012 / Published online: 9 November 2012

Abstract Herein we report the fabrication and characterization of Pd decorated Fe_3O_4 nanoparticles as highly effective catalysts for hydrogenation of 4-nitroaniline and 1,3-dinitrobenzene in liquid phase. The fabricated Fe_3O_4 nanoparticles exhibit an average size of 12 nm and super paramagnetic character with a high saturation magnetization (80 emu/g). The surface $–NH_2$ groups effectively binds the in situ formed Pd nanoparticles. Thus formed Fe_3O_4–APTES–Pd(0) catalyst showed a very high catalytic activity in reduction reactions of 4-nitroaniline and 1, 3-dinitrobenzene in liquid phase. Electron donor $–NH_2$ groups supported Pd may be responsible for the increased catalytic activity. The superparamagnetic character of this system allows easy recovery and multiple uses without significant loss of its catalytic activity.

Keywords Heterogeneous catalyst · Hydrogenation · Magnetic nanomaterials · Catalytic activity

E. Karaoglu · M. M. Summak · A. Baykal (✉)
Department of Chemistry, Faculty of Arts and Sciences, Fatih University, B.Cekmece, 34500 Istanbul, Turkey
e-mail: hbaykal@fatih.edu.tr

H. Sözeri
TUBITAK-UME, National Metrology Institute, PO Box 54, 41470 Gebze, Kocaeli, Turkey

M. S. Toprak
Division of Functional Materials, KTH-Royal Institute of Technology, Kista, 16440 Stockholm, Sweden

M. S. Toprak
Department of Materials Science and Engineering, Yildirim Beyazit University, Ulus, Ankara, Turkey

1 Introduction

Magnetic nanoparticles (MNPs)-supported catalysts have been employed as heterogeneous catalysts for various organic reactions due to their large specific surface area combined with their magnetic property [1–9]. They can easily be collected by a magnet for reuse to prevent waste of precious catalytic material. Recently, much attention has been focused on the surface modification of MNPs with appropriate capping agents to render their stability and dispersibility and to anchor the catalytically active complexes [10–14]. The MNP-supported catalysts show also a high degree of chemical stability; and, they do not swell in organic solvents. Among the known MNPs, iron oxides (Fe_3O_4 and γ-Fe_2O_3) are most commonly used as catalyst supports and in a variety of biomedical applications [15, 16]. The catalytic species can be attached onto magnetic supports either by post modification of the MNP surface [17] or by co-precipitation during the MNP synthesis [18].

Silanization agents are often considered as promising candidates for modifying the surface of iron oxide NPs directly, to increase their biocompatibility and density of the surface functional end-groups, thereby allowing further binding to other metal NPs, polymers or biomolecules [19, 20]. In general, silane-coated iron oxide NPs still exhibit the characteristic of bare iron oxide NPs; namely, maintaining a high saturation magnetization. 3-Aminopropyl-triethoxysilane (APTES), *p*-aminophenyltrimethoxysilane (APTS), and mercaptopropyltriethoxysilane (MPTES) are mostly employed for providing amino and thiol (–SH) groups on NPs. The hydroxyl groups on the iron oxide NPs surface react with the alkoxy groups of the silane molecules leading to the formation of Si–O bonds and leaving the terminal functional (amine or thiol) groups available for immobilization of other substances [21].

Heterogeneous catalysts with a matrix structure, generally known as the magnetically recyclable catalysts (MRCs), have been developed in recent years and have proved useful in separation and recovery of precious catalytic material in liquid-phase reactions by using an external magnetic field. Particularly, when the catalysts are in the nanometer size range, they possess higher activity than their pure and bulk single-metal or nonmetal counterparts [22, 23]. Therefore, the development of facile and rapid methods for the preparation of efficient MRCs is attractive. Amines have a strong affinity for noble metals (e.g. Pd, Pt) and can also keep the MNPs from aggregation, without disturbing their magnetic properties [24, 25]. Various MNP-supported Pd catalysts have been widely used for promoting organic reactions [26–31]. Pd immobilized on surface-modified Fe_3O_4/SiO_2 nanoparticles, as a magnetically separable and stable recyclable high-performance catalyst, has been developed for Suzuki and Heck cross-coupling reactions by Li and co-workers [32]. Furthermore, Pd catalyst supported by magnetically recoverable Fe_3O_4/SiO_2 has also been used for the one-pot multi-component synthesis of diazepine derivatives starting from simple and readily available precursors including a 1,2-diamine, a linear or cyclic ketone and an isocyanide [33]. Piperidine-4-carboxylic acid (PPCA)-functionalized Fe_3O_4 nanoparticles, considered as a novel organic–inorganic hybrid heterogeneous catalyst, has been fabricated and used as a magnetic catalyst for Knoevenagel reaction by Karaoglu et al. [34]. Pd decorated/coated $NiFe_2O_4$ and Fe_3O_4 MRCs were also used for hydrogenation reactions of 4-nitroaniline (NA) and 1,3-dinitrobenzene (mDNB) in the liquid phase by Karaoğlu et al. [35] and Baykal et al. [36], respectively.

In this study, we describe the preparation of superparamagnetic iron oxide nanoparticles that are coated with APTES. This organosilane can bind to the magnetite surface by covalent bonding and bind to palladium (Pd(0)) through the exposed active amino groups rendering the entire nano-assembly, (Fe_3O_4–APTES–Pd(0)), catalytically active. Detailed physicochemical characterization and catalytic activity applications in hydrogenation reaction of NA and mDNB have been performed to demonstrate the potential of the designed MRC system.

2 Experimental

2.1 Chemicals and Instrumentation

$FeCl_3{\cdot}6H_2O$, $FeCl_2{\cdot}4H_2O$, $PdCl_2$, NaOH, APTES (3-aminopropyl-triethoxysilane), and $NaBH_4$ were obtained from Merck Co. and were used without further purification.

X-ray powder diffraction (XRD) analysis was conducted on a Rigaku Smart Lab Diffractometer operated at 40 kV and 35 mA using Cu K_α radiation. High resolution transmission electron microscopy (HR-TEM) analysis was performed using a JEOL JEM 2100 microscope. Diluted sample dispersed in alcohol was drop-cast onto a Cu TEM grid and dried prior to analysis. Fourier transform infrared (FT-IR) spectra were recorded in transmission mode (Perkin Elmer BX FT-IR) on powder samples that were ground with KBr and compressed into a pellet. FT-IR spectra from 4,000 to 400 cm^{-1} were recorded to investigate the nature of the chemical bonds. The thermal stability was determined by thermogravimetric analysis (TGA, Perkin Elmer Instruments model, STA 6000). The TGA was recorded for 5 mg of powder at a heating rate of 10 °C/min from 30 to 800 °C under a nitrogen atmosphere. VSM measurements were performed by using a vibrating sample magnetometer (LDJ Electronics Inc., Model 9600). The magnetization measurements were carried out in an external field up to 15 kOe at room temperature. The optical absorption characteristics of various samples were evaluated by UV–Vis absorption spectrometry (Shimadzu UV–Vis 2600). Elemental analysis was performed using inductively coupled plasma atomic spectroscopy (Perkin Elmer Optima 4300DV ICP).

2.2 Synthetic Procedures

2.2.1 *Preparation of the Magnetic Fe_3O_4–APTES Nanoparticles (MNPs)*

Magnetic Fe_3O_4 NPs were prepared by chemical co-precipitation of chloride salts of Fe^{3+} and Fe^{2+} ions at a molar ratio of 2:1. Typically, $FeCl_3{\cdot}6H_2O$ (5.8 g, 0.02 mol) and $FeCl_2{\cdot}4H_2O$ (2.14 g, 0.01 mol) were dissolved in 100 mL deionized water at 85 °C under Ar atmosphere with vigorous stirring. (Scheme 1) Then, NaOH (10 mL, 25 %) was quickly injected into the reaction mixture in one portion. The addition of the base to the Fe^{2+}/Fe^{3+} salt solution resulted in the spontaneous formation of a black precipitate. Heating was continued for another 25-min and then the mixture was cooled to room temperature. The black precipitate was washed twice with warm distilled water. The obtained MNPs were dispersed in ethanol/water (volume ratio 1:1) solution by sonication for 30-min. Then APTES (6 mL, 99 %,) was added to the mixture. After mechanical stirring at 40 °C for 8-h, the suspended MNPs were separated magnetically. The settled product was re-dispersed in ethanol by sonication and then was isolated with magnetic decantation. This was repeated 3-times to completely remove free/unreacted APTES molecules. The precipitated product (Fe_3O_4–APTES) was dried at room temperature under vacuum.

Scheme 1 Preparation scheme for the fabrication of APTES-functionalized Fe_3O_4, Fe_3O_4–APTES, nanoparticles

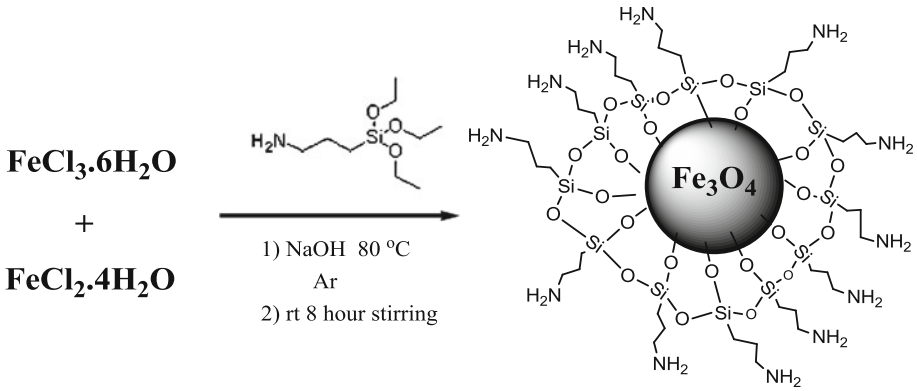

Scheme 2 Schematic representation of the formation of Fe_3O_4–APTES–Pd (0) catalyst

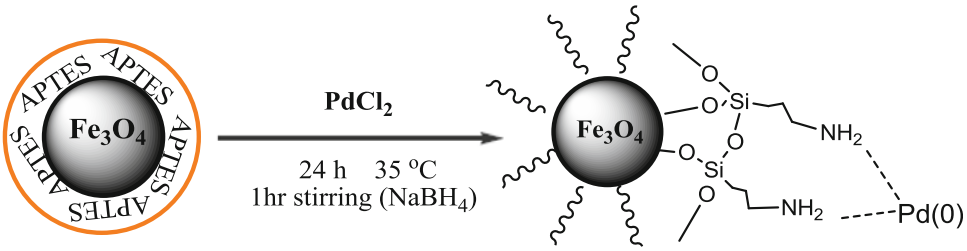

2.2.2 *Preparation of the Magnetically Recyclable Fe_3O_4–APTES–Pd(0) Catalysts (MRCs)*

The synthesized Fe_3O_4–APTES nanopowder was added to $PdCl_2$ (30 mL of 0.01 g aqueous solution) and stirred for 24-h at 35 °C. After producing Fe_3O_4–APTES–Pd^{2+}, Pd^{2+} ions were reduced by $NaBH_4$ (30 mL of 0.1 M aqueous solution), resulting in the formation of a black powder (Fe_3O_4–APTES–Pd(0)) (Scheme 2). The solid catalyst thus formed was separated by magnet and washed several times with ethanol.

2.2.3 *Catalytic Activity of MRCs on Hydrogenation of NA aniline and mDNB*

The catalytic activity of the magnetically recyclable Fe_3O_4–APTES–Pd(0) catalyst for hydrogenation of NA and mDNB by $NaBH_4$ was determined by UV–Vis spectroscopy. Specifically, by comparing the decrease in the intensity of the characteristic band at 380 nm (originating from the $–NO_2$ group) for NA and ~240 nm for m-DNB. The absorption spectra of the reaction solution were recorded at different times after the addition of the catalyst.

According to the ICP results, the Pd content in the product was 3.5 % by weight. In a typical run, 0.2 mL magnetically recyclable aqueous Fe_3O_4–APTES–Pd(0) catalyst solution with a Pd concentration of 0.1 mg/mL was added to a mixture of NA (1.4 mL 0.4 mM) or mDNB, and $NaBH_4$ (1.4 mL, 30 mM). The molar ratio of Pd to NA/mDNB was kept at approximately 1:2 during the reaction.

3 Results and Discussion

3.1 XRD Analysis

Phase investigation of the crystallized product was performed by XRD. The powder diffraction pattern of the APTES-coated nanoparticles is presented in Fig. 1. All the observed diffraction peaks were indexed to the cubic structure of Fe_3O_4 (JCPDS no. 19-629) revealing the high phase purity of the product. The diffraction peaks were

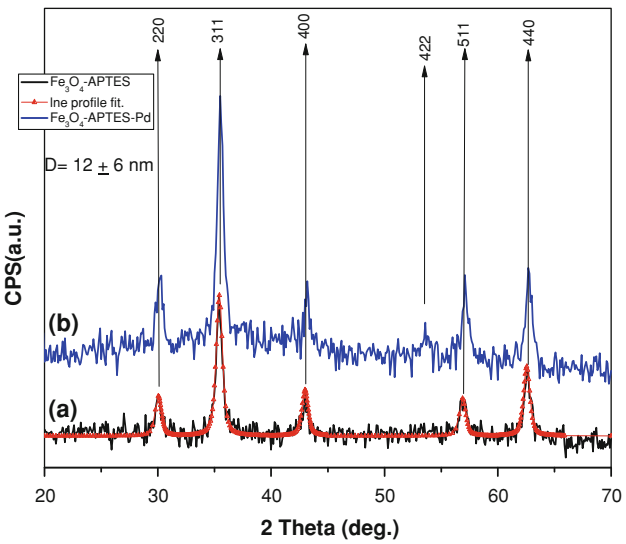

Fig. 1 XRD powder diffraction pattern of **a** Fe_3O_4–APTES and **b** Fe_3O_4–APTES–Pd(0) with their line profile fitting

broadened owing to very small crystallite size. The mean crystallite size was estimated from the diffraction pattern by the line profile fitting method using the Eq. 1 given in Ref. [37, 38]. The line profile (Fig. 1) was fitted for the observed seven peaks with the following miller indices: (220), (311), (222), (400), (422), (511) and (440). The average crystallite size obtained is 12 ± 6 nm.

3.2 FT-IR Analysis

The FT-IR spectra of uncoated Fe_3O_4 NPs and Fe_3O_4–APTES–Pd(0) catalyst are shown in Fig. 2. The spectrum of the Fe_3O_4 NPs (Fig. 2a) exhibits a metal–oxygen band, v_1, at 590 cm^{-1} corresponding to intrinsic stretching vibrations of the metal at a tetrahedral site ($Fe_{tetra} \leftrightarrow O$), whereas the metal–oxygen band observed at 445 cm^{-1}, v_2, is assigned to an octahedral-metal stretching ($Fe_{octa} \leftrightarrow O$) [39–44].

The adsorption of APTES onto the surface of magnetite particles was confirmed by bands at 1110, 1050 and 990 cm^{-1} assigned to the SiO–H and Si–O–Si groups [45, 46]. The silica network was bonded to the magnetite surface by Fe–O–Si bonds. This absorption band cannot be seen in the FT-IR spectrum because it appears at ~584 cm^{-1}, which overlaps with the Fe–O vibration of the magnetite nanoparticles [47, 48]. The absorption bands at 922 and 862 cm^{-1} revealed the presence of Si–O–H and OH vibrations on the surface of the magnetite. The two broad bands at 3,417 and 1,625 cm^{-1} are ascribed to the N–H stretching and NH_2 bending vibrations of free NH_2 group, respectively [49, 50]. At ~3,400 cm^{-1}, the symmetric and asymmetric –NH stretch modes of amino groups in APTES are very weak. Absorption bands at 2929, 1313 and 924 cm^{-1} are associated with the vibration bands for $–CH_2$, C–N and $Si–CH_2$ bonds, respectively, from aminopropylsilane [51]. The presence of C–H was confirmed by the stretching vibrations at 2,930 and 2,862 cm^{-1} [52–56]. For the APTES-coated nanoparticles, Si–O–Si stretching was verified by the absorption bands at 1,150–1,100 cm^{-1} [57]. Thus, the surface of the MNPs were successfully functionalized with amino groups by this synthetic process, and is in agreement with the earlier reports [20, 25].

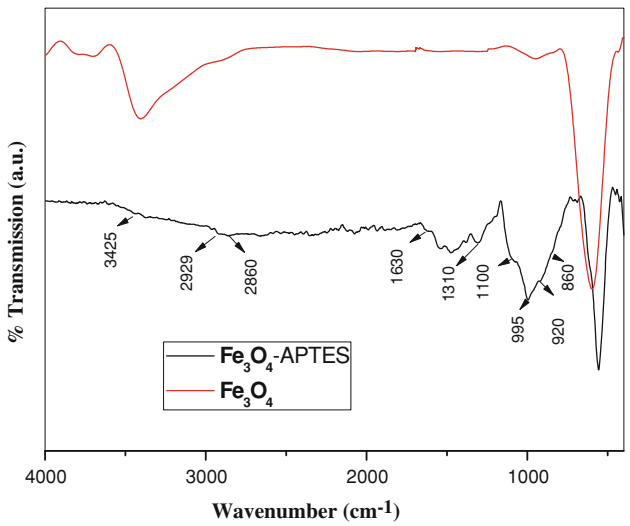

Fig. 2 The FT-IR spectra of **a** uncoated Fe_3O_4 NPs, **b** Fe_3O_4–APTES catalyst

3.3 TEM Analysis

The morphology of the Fe_3O_4–APTES–Pd(0) catalyst along with a size distribution histogram are determined by TEM. The micrographs are given in Fig. 3. Particles were observed to have a mixture of polygonic and spherical morphology. A closer examination of Fe_3O_4 NPs (Fig. 3b) reveals the presence of very small (<1 nm) Pd particles with a darker contrast due to their high density. This also indicates that functionalization and subsequent reduction to decorate the Pd NPs on the Fe_3O_4 NPs was successfully achieved. The average size of Fe_3O_4–APTES NP was estimated at 12 ± 2 nm. The size estimated from TEM micrographs agrees well with the crystallite size estimated from XRD line profile fitting, which may reveal the nearly single crystalline character of Fe_3O_4 NPs.

3.4 Thermal Analysis

The thermal stability of the Fe_3O_4–APTES–Pd(0) catalyst was evaluated by TG. The thermograms are given in Fig. 4. The values of the residual weights were used to assess the APTES content in the material. Upon heating, the magnetite NPs showed a weight loss of ~2 % fom 65 to 130 °C and is mainly due to the loss of physically adsorbed water. The weight loss of APTES-modified magnetite NPs is 16 % over a broad temperature range of 250–700 °C [56, 58], which reveals the composition of the material as 82 % MNP and 16 % APTES.

3.5 Magnetization Measurements

The room temperature magnetization curve for the Fe_3O_4–APTES–Pd(0) catalyst is given in Fig. 5. The M-H hysteresis curve has a negligible coercivity and remanence. In addition, magnetization of the sample increases with the external magnetic field without reaching saturation even at 1.5 T. These are characteristic features of super-paramagnetic NPs. Specific saturation magnetization, M_s, of the sample is 63 emu/g at 15 kOe. However, this value should be normalized to the weight of the magnetic core (ca. 82 %). M_s of Fe_3O_4–APTES–Pd(0) catalyst reaches 75.5 emu/g upon normalization, which is still far from the theoretically predicted value (i.e., 92 emu/g). The possible reason for this observation in nanoparticle systems is the

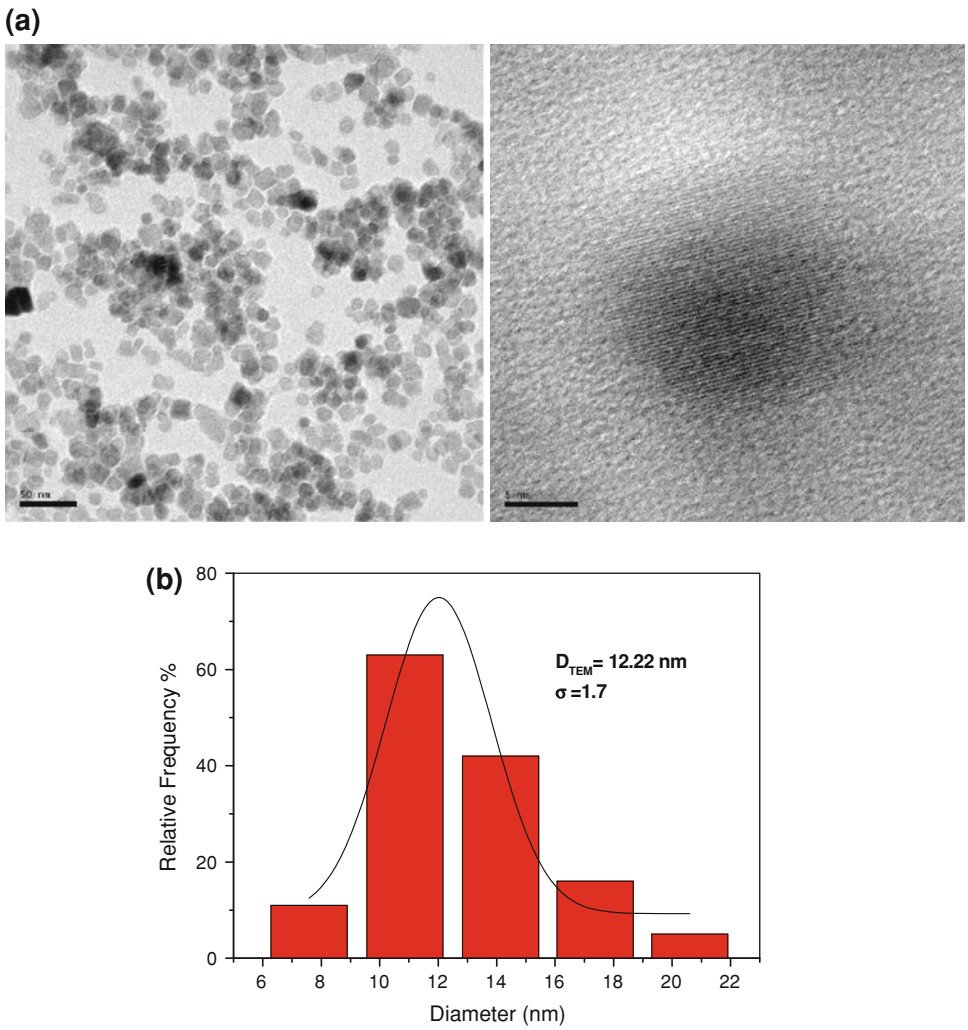

Fig. 3 **a** The TEM micrographs of Fe_3O_4–APTES–Pd(0) catalyst at different magnifications, **b** Size distribution histogram obtained from the micrographs in (**a**)

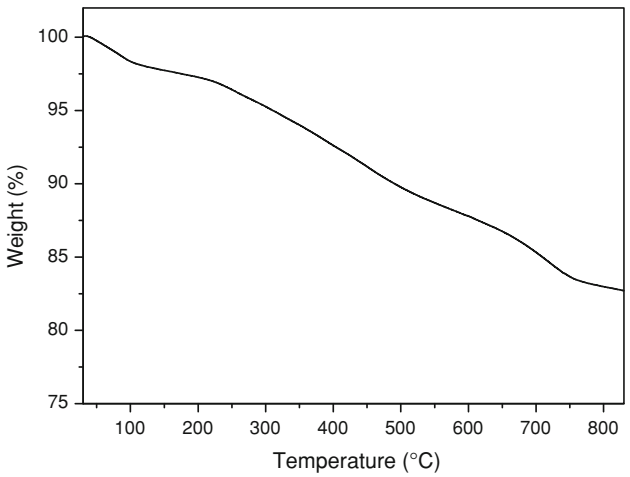

Fig. 4 TG thermogram of Fe_3O_4–APTES–Pd(0) catalyst

difference in spin ordering at the surface of the particles over that in the bulk, which forms a magnetic core non-magnetic shell configuration. Surface effects dominate the properties of the nanoparticles since decreasing the particle size increases the surface-to-core spin ratio. Surface effects result from the lack of translational symmetry at the boundaries of the particle due to the lower coordination number and existence of broken magnetic exchange bonds that lead to the surface spin disorder and frustration. The magnetization of the Fe_3O_4–APTES–Pd(0) catalyst is further reduced most probably by the presence of the surfactant molecules on the surface of the magnetite core. This occurs over the O-atoms on the surface of the SPIONs. Some of the free electrons; i.e., magnetic moments, are used in this process. Hence, the reduced M_s can be ascribed to surface spin disorder, canting and adsorption of surfactant molecules to the surface of the SPIONs [59, 60].

Magnetization of the Fe_3O_4–APTES–Pd(0) catalyst can be described by the Langevin function (Eq. 1), which can be used to determine the magnetic domain size,

$$M = M_s\left\{\coth\left(\frac{\mu H}{k_B T}\right) - \frac{k_B T}{\mu H}\right\} \quad (1)$$

where, μ denotes the mean magnetic moment of a single particle, H is applied field and $k_B T$ corresponds to the thermal

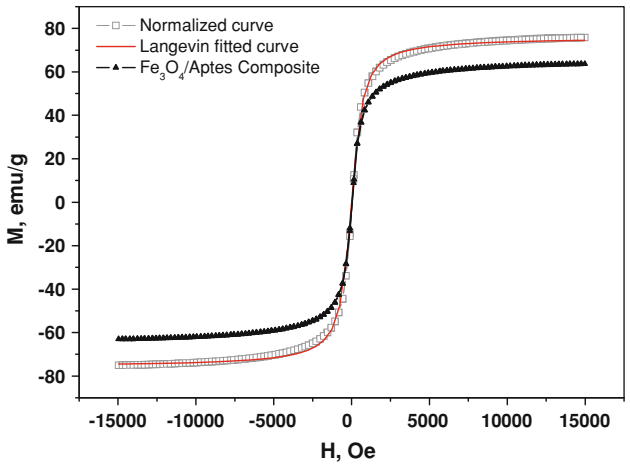

Fig. 5 Room temperature M–H hysteresis curve of Fe_3O_4–APTES–Pd(0) catalyst and bulk magnetite, which is determined by normalization of the former curve to the mass fraction of the magnetic core. The solid line corresponds to a Langevin fit of the measured M-H hysteresis curve and is used to determine average magnetic domain size

energy of the particles. The Langevin relation considers each particle as a magnetic mono-domain. The relationship between the mean magnetic moment of a particle and saturation magnetization of system of particles (Eq. 2) can be used to calculate average magnetic domain size, D,

$$\mu = \frac{M_s \pi \rho D^3}{6} \tag{2}$$

where ρ is the density of the sample.

The mean magnetic moment, which is used as a fitting parameter, is determined by fitting Eq. 1 to the *M-H* hysteresis curve of the composite that is normalized to the bulk mass as 15.305 μ_B at 300 K. Using this value, the mean magnetic domain size; i.e., 8.96 ± 1.00 nm, is obtained. The magnetic domain size is slightly smaller than the average crystallite size and particle size, which is estimated from XRD and TEM analyses. This also confirms the presence of a magnetically dead layer on the Fe_3O_4 NPs.

3.6 Catalytic Activity

3.6.1 Catalytic Activity of MRCs on Hydrogenation of NA

During hydrogenation, the band at 380 nm originating from the $–NO_2$ group decreases in intensity and a new band appears at ~240 nm, which arises from the formation of

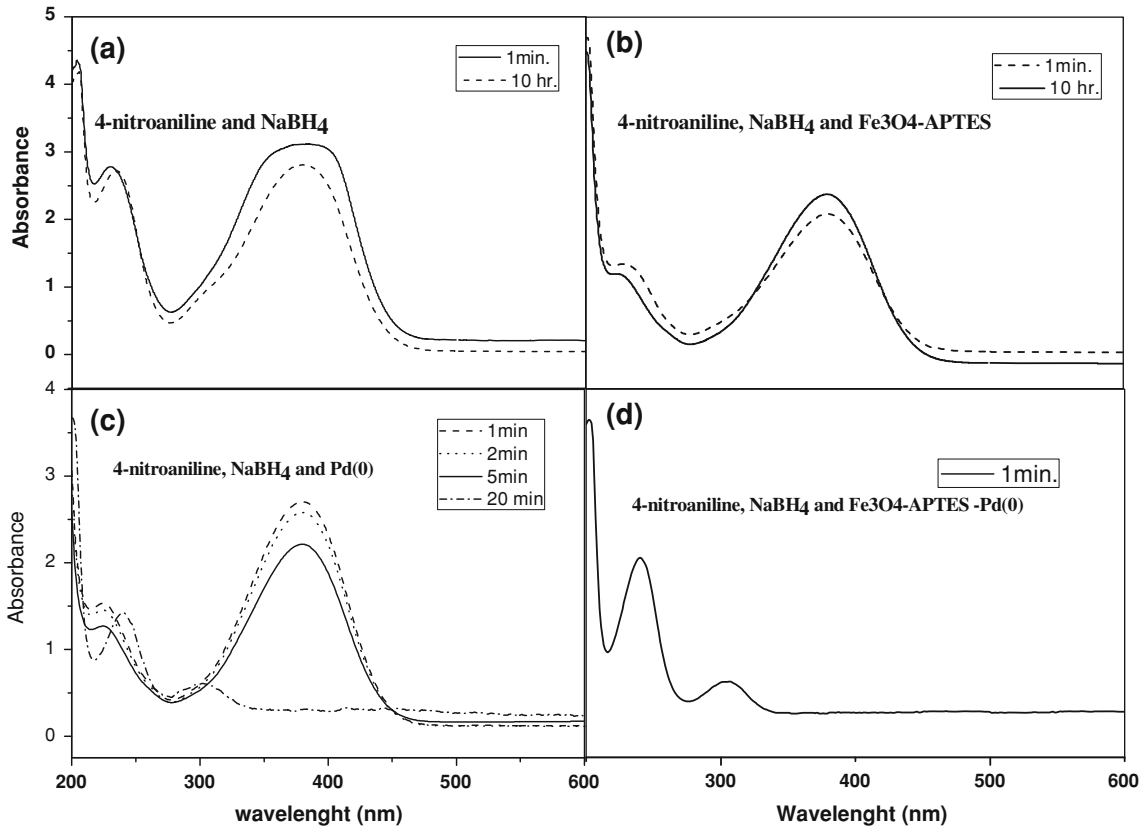

Fig. 6 Absorption spectra of 4-nitroaniline and **a** $NaBH_4$ mixed aqueous solution after 1-min and 10-h, **b** Fe_3O_4–APTES NP mixed aqueous solution after 1 min and 10 h, **c** Pd(0) catalyst mixed aqueous solution in different time intervals, **d** Fe_3O_4–APTES–Pd(0) catalyst mixed aqueous solution after 1 min

4-phenylenediamine. The formation of this compound confirms complete hydrogenation of NA.

The hydrogenation of NA by $NaBH_4$ in the absence of catalyst was quite slow. The spectra of the mixture of NA and $NaBH_4$ solutions (Fig. 6a) was dominated by the band at 380 nm, which corresponds to intermolecular charge transfer for NA [61]. The intensity of this characteristic band decreases very slowly after 1-h. The catalytic effect of the Fe_3O_4–APTES nanocomposite on the hydrogenation of NA was also investigated. It was found that it had very little effect (Fig. 6b). On the other hand, the hydrogenation of NA was greatly accelerated after the addition of an aqueous solution of the Fe_3O_4–APTES–Pd(0) catalyst (Fig. 6d). The successive absorption spectra are shown in Fig. 6d. In the presence of the Fe_3O_4–APTES–Pd(0) catalyst, the reaction reaches completion after only 1.0-min.

Comparatively, after the addition of an aqueous solution of Pd(0), the reduction peak disappears after 20-min (Fig. 6c). The results indicate that the catalytic activity of the magnetically recyclable Fe_3O_4–APTES–Pd(0) catalyst is better than that of the Pd/C catalyst. This may be due to the fact that in Fe_3O_4–APTES–Pd(0), the Pd NPs were evenly decorated on NH_2 (Scheme 1), where N acts as electron donor increasing the activity of Pd. As a result, the magnetically recyclable Fe_3O_4–APTES–Pd(0) catalysts offer higher catalytic activity by accelerating electron transfer from $NaBH_4$ to Pd NPs on the MRCs and finally to NA.

The reusability of the magnetic catalyst was also examined by carrying out five repeated runs using the same batch of recycled ~2 mol% Fe_3O_4–APTES–Pd(0) catalyst in hydrogenation. The decrease in the activity of the catalyst after five runs is only 3 %, which indicates that multiple use (after recycling) without significant loss of material and catalytic activity is possible (Fig. 7).

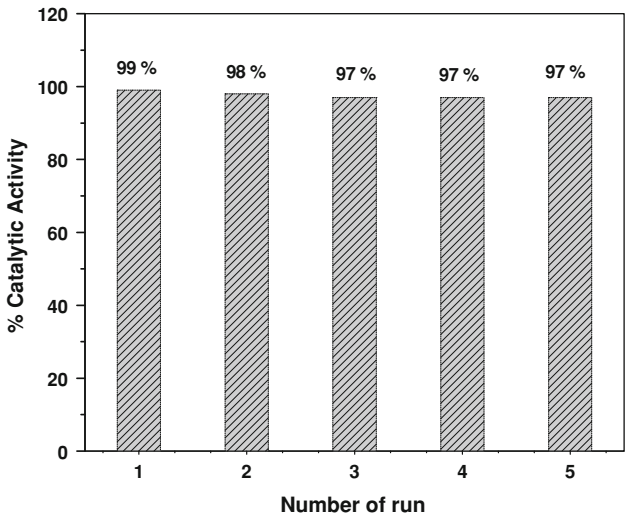

Fig. 7 Repetitive use versus catalytic activity of Fe_3O_4–APTES–Pd(0) catalyst

3.6.2 *Catalytic Activity of MRCs on Hydrogenation of mDNB*

The catalytic activity test of Fe_3O_4–APTES–Pd(0) on the hydrogenation of mDNB was also performed by observing the absorption peak of mDNB at ~240 nm [62]. The hydrogenation reaction that took ~10-h in the presence of $NaBH_4$ took only 1-min in the presence of Fe_3O_4–APTES–Pd(0) (data not shown) [63]. This indicates the versatility and high catalytic activity of the MRC for hydrogenation reactions in the liquid phase (Fig. 8).

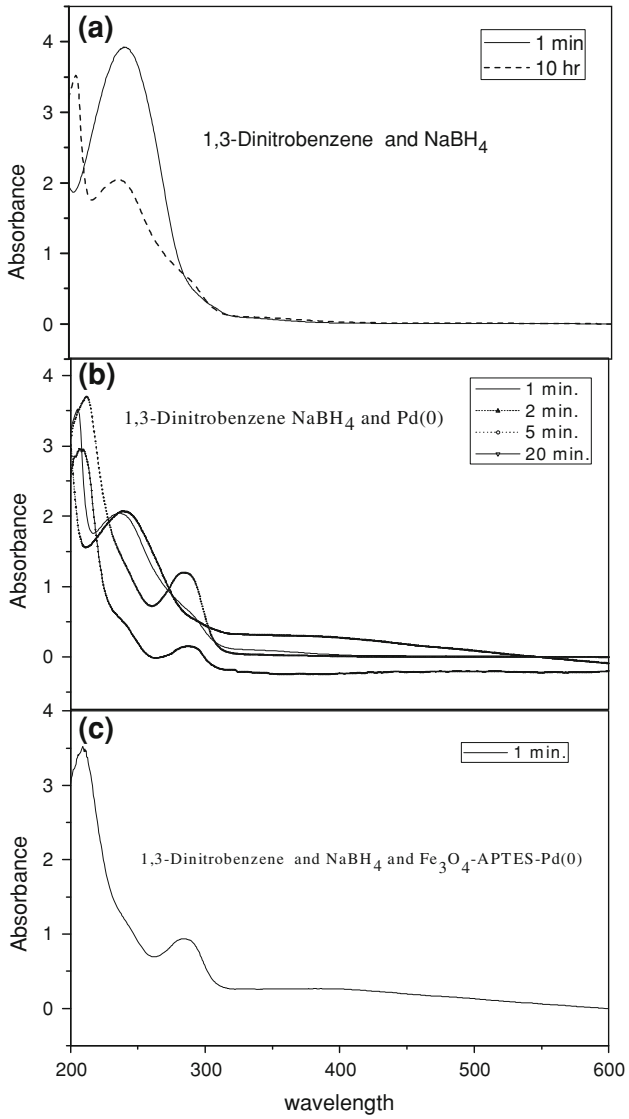

Fig. 8 Absorption spectra of 1,3-Dinitrobenzene and **a** $NaBH_4$ mixed aqueous solution after 1 min and 10 h, **b** Fe_3O_4–APTES nanocomposite mixed aqueous solution after 1, 2, 5 and 20 min, **c** Fe_3O_4–APTES–Pd(0) catalyst mixed aqueous solution after 1 min

4 Conclusion

The fabrication and characterization of Pd-decorated Fe_3O_4 nanoparticles as a highly effective catalyst for reduction reactions in liquid phase was developed. The nanoparticles were characterized by FT-IR, XRD, TEM, TGA, ICP, UV–Vis and VSM techniques. The fabricated Fe_3O_4 nanoparticles exhibited an average size of 12 nm (TEM, X-ray line profile fitting), and a magnetic domain size of 9 nm, which reveal a nearly single crystalline character of the nanoparticles as well as the presence of a magnetically dead layer. Superparamagnetic character with a high saturation magnetization (80 emu/g) make this material attractive since it is now possible to easily recover the catalysts from solution after use by magnetic decantation. FT-IR analysis confirms the presence of APTES coating with exposed amine ($–NH_2$) groups on the nanoparticles. These $–NH_2$ groups were effective in binding in situ formed Pd nanoparticles. The fabricated Fe_3O_4–APTES–Pd(0) catalyst showed very high catalytic activity in the reduction of NA and mDNB in the liquid phase. Electron donor $–NH_2$ groups may be responsible for the increased catalytic activity of the supported Pd nanoparticles. The magnetic character of this system allowed recovery and multiple uses without significant loss of its catalytic activity.

Acknowledgments This work is supported by Fatih University under BAP Grant no P50021104-B.

References

1. L. Zhou, C. Gao, W. Xu, Langmuir **26**, 11217 (2010)
2. J.M. Thomas, B.F.G. Johnson, R. Raja, G. Sankar, P.A. Midgley, Acc. Chem. Res. **36**, 20 (2003)
3. Y. Zhu, L.P. Stubbs, F. Ho, R. Liu, C.P. Ship, J.A. Maguire, N.S. Hosmane, ChemCatChem **2**, 365 (2010)
4. V. Polshettiwar, R.S. Varma, Org. Biomol. Chem **7**, 37 (2009)
5. S. Shylesh, V. Schünemann, W.R. Thiel, Angew. Chem. Int. Ed **49**, 3428 (2010)
6. M. Kawamura, K. Sato, Chem. Commun. **45**, 4718 (2006)
7. C.W. Lim, I.S. Lee, Nano Today **5**, 412 (2010)
8. K. Tanaka, Catal. Today **154**, 105 (2010)
9. V. Polshettiwar, B. Baruwati, R.S. Varma, Green Chem. **11**, 127 (2009)
10. D. Guin, B. Baruwati, S. Manorama, Org. Lett. **9**, 1419 (2007)
11. K.S. Lee, M.H. Woo, H.S. Kim, E.Y. Lee, I.S. Lee, Chem. Commun. **25**, 3780 (2009)
12. Z. Wang, B. Shen, Z. Aihua, N. He, Chem. Eng. J. **113**, 27 (2005)
13. J. Zhou, R. Zhou, L. Mo, S. Zhao, X. Zheng, J. Mol. Catal. A Chem. **178**, 289 (2002)
14. V. Polshettiwar, Á. Molnár, Tetrahedron **63**, 6949 (2007)
15. L.M. Rossi, I.M. Nangoi, N.J.S. Costa, Inorg. Chem. **48**, 4640 (2009)
16. Z. Wang, P. Xiao, B. Shen, N. He, Colloids Surf. A **276**, 116 (2006)
17. H. Erdemi, A. Baykal, E. Karaoğlu, M.S. Toprak, Mater. Res. Bull. **47**, 2193 (2012)
18. A.H. Lu, E.L. Salabas, F. Schuth, Angew. Chem. Int. Ed. **46**, 1222 (2007)
19. X. Shen, X. Fang, Y. Zhou, H. Liang, Chem. Lett. **33**, 1468 (2004)
20. M. Ma, Y. Zhang, W. Yu, H. Shen, H. Zhang, N. Gu, Colloid Surf. A **212**, 219 (2003)
21. W. Wu, Æ Q. He, Æ C. Jiang, Nanoscale Res. Lett . **3**, 397 (2008)
22. C.W. Lim, I.S. Lee, Nano Today **5**, 412 (2010)
23. M.D. Kaminski, L. Nuñez, J. Magn. Magn. Mater. **194**, 31 (1999)
24. D. Yi, S. Lee, J. Ying, Chem. Mater. **18**, 2459 (2006)
25. M. Ma, Q. Zhang, D. Yin, J. Dou, H. Zhang, H. Xu, Catal. Commun. **17**, 168 (2012)
26. K.K. Senapati, S. Roy, C. Borgohain, P. Phukan, J. Mol. Catal. A Chem. **352**, 128 (2012)
27. S.C. Tsang, V. Caps, I. Paraskevas, D. Chadwick, D. Thompsett, Angew. Chem. Int. Ed. **43**, 5645 (2004)
28. J. Liu, X. Peng, W. Sun, Y. Zhao, C. Xia, Org. Lett. **10**, 3933 (2008)
29. L.M. Rossi, F.P. Silva, L.L.R. Vono, P.K. Kiyohara, E.L. Duarte, R. Itri, R. Landers, G. Machado, Green Chem. **9**, 379 (2007)
30. Z. Gao, Y. Feng, F. Cui, Z. Hua, J. Zhou, Y. Zhu, J. Shi, J. Mol. Catal. A Chem. **336**, 51 (2011)
31. Z. Wang, P. Xiao, B. Shen, N. Hea, Colloids Surf. A physicochem Eng. Aspects **276**, 116 (2006)
32. Q. Du, W. Zhang, H. Ma, J. Zheng, B. Zhou, Y. Li, Tetrahedron **68**, 3577 (2012)
33. A. Maleki, Tetrahedron **68**, 7827 (2012)
34. E. Karaoglu, A. Baykal, M. Senel, H. Sozeri, M.S. Toprak, Mater. Res. Bull. **47**, 2480 (2012)
35. E. Karaoğlu, U. Özel, C. Caner, A. Baykal, M.M. Summak, H. Sözeri, Mater. Res. Bull. **47**, 4316 (2012)
36. A. Baykal, E. Karaoglu, H. Sözeri, E. Uysal, M.S. Toprak, J. Supercond. Novel Magn. (2012). doi:10.1007/s10948-012-1702-2
37. T. Wejrzanowski, R. Pielaszek, A. Opalinska, H. Matysiak, W. Łojkowski, K.J. Kurzydłowski, Appl. Surf. Sci. **253**, 204 (2006)
38. R. Pielaszek, *Analytical expression for diffraction line profile for polydispersive powders, Appl. Crystallography* (Proceedings of the XIX Conference, Krakow, 2003), p. 43
39. B. Garlyyev, Z. Durmus, N. Kemikli, H. Sozeri, A. Baykal, R. Ozturk, Polyhedron **30**, 2843 (2011)
40. E. Temizel, E. Aya, M. Senel, H. Erdemi, M.S. Yavuz, H. Kavas, A. Baykal, R. Öztürk, Mater. Chem. Phys. **131**, 284 (2011)
41. M. Aydın, B. Ünal, B. Esat, A. Baykal, E. Karaoglu, M.S. Toprak, H. Sözeri, J. Alloys Compd. **514**, 45 (2012)
42. H. Deligöz, A. Baykal, M. Senel, H. Sözeri, E. Karaoglu, M.S. Toprak, Synth. Met. **162**, 590 (2012)
43. E. Karaoglu, A. Baykal, H. Erdemi, L. Alpsoy, H. Sozeri, J. Alloys Compd. **509**, 9218 (2011)
44. R.D. Waldron, Phys. Rev. B **99**, 1727 (1955)
45. L.D. White, C.P. Tripp, J. Colloid Interface Sci. **232**, 400 (2000)
46. R.A. Bini, R.F.C. Marques, F.J. Santos, J.A. Chaker, M. Jafelicci Jr., J. Magn. Magn. Mater. **324**, 534 (2012)
47. L.G. She, L.L. Ping, R.L. Smith Jr, H. Inomata, J. Mol. Struct. **560**, 87 (2001)
48. S. Bruni, F. Cariati, M. Casu, A. Lai, A. Musinu, G. Piccaluga, S. Solinas, Nanostruct. Mater. **11**, 573 (1999)
49. L.D. White, C.P. Tripp, J. Colloid Interface Sci. **232**, 400 (2000)
50. Z. Xu, Q. Liu, J.A. Finch, Appl. Surf. Sci. **120**, 269 (1997)
51. B.C. Simionescu, J. Magn. Magn. Mater. **324**, 1679 (2012)
52. M. Yamauraa, R.L. Camiloa, L.C. Sampaiob, M.A. Macedoc, M. Nakamurad, H.E. Toma, J. Magn. Magn. Mater. **279**, 210 (2004)
53. Y.L. Wua, J.J. Lin, P.Y. Hsua, C.P. Hsu, Sens. Actuators B **155**, 709 (2011)
54. G. Tan, L. Zhang, C. Ning, X. Liu, J. Liao, Thin Solid Films **519**, 4997 (2011)
55. H. Sardon, L. Irusta, M.J. Fernández-Berridi, M. Lansalot, E. Bourgeat-Lami, Polymer **51**, 5051 (2010)

56. K. Can, M. Ozmen, M. Ersoz, Colloids Surf. B **71**, 154 (2009)
57. S. Bruni, F. Cariati, M. Casu, A. Lai, A. Musinu, G. Piccaluga, S. Solinas, Nanostruct. Mater. **11**, 573 (1999)
58. A.D. Angheluta, A. Dascalu, A. Fifere, A. Coroaba, L. Pricop, H. Chiriac, V. Tura, M. Pinteala, B.C. Simionescu, J. Magn. Magn. Mater. **324**, 1679 (2012)
59. X. Batlle, A. Labarta, J. Phys. D Appl. Phys. **35**, 15 (2002)
60. R.H. Kodama, A.E. Berkowitz, E.J. McNiff Jr, S. Foner, Phys. Rev. Lett. **77**, 394 (1996)
61. L. Kong, X. Lu, E. Jin, S. Jiang, X. Bian, W. Zhang, C. Wang, J. Solid State Chem. **182**, 2081 (2009)
62. K. Sharmaa, S.C. Lahiri, Spectrochim Acta Part A **79**, 1063 (2011)
63. P. Nalawade, T. Mukherjee, S. Kapoor, Colloids Surf. A physicochem Eng. Aspects **396**, 336 (2012)